Electrochemical impedance spectroscopy of iron corrosion in H 2 S solutions

Martien Duvall Deffo Ayagou, Mai Tran, Bernard Tribollet, Jean Kittel, Eliane Sutter, Nicolas Ferrando, Christophe Mendibide, Claude Duret-Thual

Electrochemical impedance spectroscopy of iron corrosion in H_2S solutions

Martien Duvall Deffo Ayagou[1,2], Thi Tuyet Mai Tran[3], Bernard Tribollet[3], Jean Kittel[1*], Eliane Sutter[3], Nicolas Ferrando[4], Christophe Mendibide[2], Claude Duret-Thual[2].

1- IFP Energies nouvelles, Rond-Point de l'échangeur de Solaize ,BP3, 69360 Solaize, France

2- Institut de la Corrosion – Site de Saint-Etienne, zone d'activités du parc secteur Gampille 42490 Fraisses, France

3- Sorbonne Université, CNRS, Laboratoire Interfaces et Systèmes Electrochimiques (LISE), F-75005 Paris, France

4- IFP Energies nouvelles 1 et 4 avenue de Bois-Préau 92852 Rueil-Malmaison, France

** corresponding author: **jean.kittel@ifpen.fr***

Abstract

Corrosion of iron exposed to H_2S saturated solution at pH 4 was studied by electrochemical impedance spectroscopy, weight loss coupons and surface analysis. Hydrogen permeation was also used as indirect means of evaluating the intensity of the proton reduction reaction leading to hydrogen entry into the metal.

Since corrosion in this type of test solution results in the rapid build-up of a conductive and highly porous iron sulfide scale, a specific contribution of the film has to be considered. An impedance model was thus proposed. The faradaic anodic impedance consists of a two-step reaction with charge transfer and adsorption – desorption. An additional contribution, associated with the conductive and highly porous iron sulfide film was added in parallel. This contribution, mostly visible in the

low frequency domain, presents a 45° tail associated with a porous electrode behavior. This model was well adapted to describe impedance diagrams measured at various exposure times, up to 620 hours. Charge transfer resistance determined from impedance analysis allowed calculating the evolution with time of the corrosion current density. A very good correlation was found between this corrosion current density and the hydrogen permeation current density. As expected in our experimental conditions, a permeation efficiency close to 100 % is demonstrated. Corrosion rate of 490 µm/year was measured by weight-loss specimens, confirming the validity of the impedance analysis, which resulted in a calculated corrosion rate of 530 µm/year.

keywords : Corrosion, iron, H_2S, EIS, porous electrode

1. Introduction

Corrosion of metallic materials in the oil and gas industry has been a significant concern over the last decades and has major financial and environmental implications. H_2S and CO_2 are two main corrosive agents in the oil and gas industry. Several studies have been carried out to understand the corrosion of steel in a CO_2 medium, and there is a relative consensus on the mechanisms, which are often related to the formation of an iron carbonate scale. Depending on the conditions, such scale may have a protective action through a blocking effect, or provide no protection at all. Electrochemical impedance spectroscopy (EIS) represents an interesting technique to study the evolution with time of corrosion reaction, as it is usually performed at the corrosion potential. Most EIS studies of CO_2 corrosion were conducted at ambient temperature and in NaCl solutions saturated with CO_2 at

atmospheric pressure [1–5]. Typical impedance diagrams contain a high frequency (HF) capacitive loop followed by an inductive loop at low frequency (LF). The HF loop has typical resistance value of several hundreds of Ω.cm² and a characteristic frequency of a few hertz, corresponding to a capacitance around 100 µF/cm². This capacitance value is typical of the double-layer at a bare metal surface [6]. It is also well admitted that the resistive component corresponds to the charge transfer associated with the faradaic response [3,4]. The inductive behavior at low frequency is often attributed to relaxation of intermediate adsorbates [3,7]. The low frequency behavior seems however less reproducible, as some studies also showed a capacitive loop in the mHz frequency domain instead of the inductive loop [3].
Similar shapes of impedance curves were obtained in CO_2 environments with traces of H_2S at concentrations up to at least 100 ppm vol. with respect to CO_2 [1,2]. Unfortunately, it was not possible to extract capacitance values from these publications, since Nyquist plots did not include characteristic frequencies.
It results from all these studies that low alloy steel corrosion in CO_2 saturated solution at ambient temperature results in a capacitive loop associated with the charge transfer resistance in parallel with the double layer capacitance. An additional contribution, either inductive or capacitive can also be observed at lower frequencies, in the mHz domain.

Compared to CO_2, electrochemical measurements in H_2S environments seem to be much more difficult, and the shape of impedance diagrams vary a lot between various studies.
Ma et al. published several papers on pure iron exposed to H_2SO_4 / Na_2SO_4 solutions with dissolved H_2S introduced as Na_2S [8,9]. In these studies, pH range varied from

0.7 to 3.5, and dissolved H_2S concentration was 0.4 mmol/L, corresponding to the equilibrium with gaseous H_2S at a partial pressure of 4 mbar. Impedance diagrams measured at the corrosion potential showed two capacitive loops, and were interpreted with the equivalent circuit shown in Figure 1.a. In this circuit, CPE_{dl} and R_t were respectively attributed to the double layer capacitance and charge transfer resistance, corresponding to the HF capacitive loop. R_t values between 13 and 72 $\Omega.cm^2$ and C_{dl} values between 25 and 140 $\mu F.cm^{-2}$ were derived from equivalent circuit fitting. CPE_a and R_a are associated with relaxation of adsorbed species, which was supposed to proceed slower and to correspond to the LF arc. These authors also measured impedance diagrams at various anodic potentials in order to promote the anodic reaction versus the cathodic contribution [8,9]. At the more anodic potentials, an inductive loop appeared at low frequency. This led the authors to use another equivalent circuit, claimed to represent anodic dissolution (Figure 1.b). Although they look quite different, it can be shown that both circuits of Figure 1.a and b correspond to a similar analytical expression of the impedance of anodic dissolution through an adsorbed intermediate [10]. For such system, and depending on surface coverage and constant parameter values, the low frequency contribution may correspond either to a capacitive arc (Figure 1.a) or to an inductive loop (Figure 1.b). The same equivalent circuit as Figure 1.a was used by Veloz et al. to describe experimental results on mild steel exposed to a brine (30 g/L NaCl) solution buffered at pH 3.5 by sodium acetate and acetic acid, saturated by 1 bar dissolved H_2S (0.1 mol/L) [11]. Tests were performed for short exposure times, after which no iron sulfide or any other corrosion product layer was detected by XRD analysis. In these conditions, charge transfer resistance in the order of 150 $\Omega.cm^2$ and a double layer capacitance of 60 $\mu F.cm^{-2}$ were measured.

A last study used the same equivalent circuit (Figure 1.a) for the interpretation of impedance data in H_2S [12]. Similarly to the studies by Ma et al., test solutions were prepared with H_2SO_4 and Na_2SO_4, and H_2S was introduced as Na_2S. However, temperature was raised to 90 °C, while all previous studies were conducted at ambient temperature. Impedance plots obtained in presence of H_2S at the corrosion potential consisted of two capacitive loops. R_t and C_{dl} values were extracted by curve fitting with the equivalent circuit of Figure 1.a. The values of the double layer capacitance presented in this paper were of the order of mF/cm^2 which is much higher than expected values for a double layer capacitance, in the order of ten to a few hundred µF/cm^2 [6,12]. The reasons for such high values were not commented.

Significantly different shapes of impedance results were obtained by Arzola et al. [13]. They performed tests in 30 g/L NaCl solutions with various H_2S concentrations ranging from 100 mass ppm to 2550 mass ppm (i.e. corresponding to equilibrium with 30 mbar to 700 mbar H_2S). pH of test solutions varied from 5.3 (for 100 ppm H_2S) to 4.1 (2550 ppm H_2S). Measurements were performed immediately after immersion, and repeated after 24 hours exposure. Impedance diagrams were quite different from those obtained by previous authors. They consisted of a capacitive loop at high frequency interpreted by the charge transfer resistance in parallel to the double layer capacitance, followed by a 45° tail at low frequency assumed to represent a diffusion process (Figure 1.c). R_{ct} values immediately after immersion were comprised between 300 Ω.cm^2 at the higher H_2S content and 1315 Ω.cm^2 at 100 ppm H_2S. These values increased respectively to 460 Ω.cm^2 and 2060 Ω.cm^2 after 24 hours exposure. Unfortunately, capacitance values were not reported in the paper, and since no frequency information was given in the Nyquist plots, it was also impossible

to evaluate these values from the frequency at the maximum of the imaginary part of the impedance. The low frequency contribution (45° tail) was not analyzed in the paper. It was just stated that it could correspond to diffusion through the iron sulfide film formed at the metal surface.

In summary, two different impedance shapes are presented in available literature on H_2S corrosion of low alloy steels. The first type of results shows a HF behavior dominated by the anodic charge transfer resistance and the double layer capacitance, while low frequency characteristics correspond to relaxation of adsorbed species (Figure 1.a and 1.b). This type of result was obtained for short immersion times, and it was mentioned that no surface precipitation was visible after the tests. Indeed, these tests were performed at low pH or in presence of acetate, which retards iron sulfide precipitation. In that case, impedance response is mainly dominated by anodic reactions.

The second type of result shows a different behavior, with a 45° tail at low frequency, interpreted by diffusion limitation (Figure 1.c). In that case, presence of iron sulfide scale was observed. In addition, impedance measurements were performed at short immersion time and then repeated after 24 hours, and a significant increase of the high frequency semi-circle (interpreted as R_t) was observed, and was associated with a decrease of the corrosion rate.

Figure 1: Equivalent circuits and corresponding impedance diagram used in the literature to describe iron corrosion in presence of H_2S [8,9,13]. For the sake of simplicity, electrolyte resistance was removed from these equivalent circuits.

The first aim of this paper is thus to examine the evolution with time of EIS spectra of pure iron exposed to water containing dissolved H_2S. Contrary to what already exists in the literature, time evolution over a few weeks will be examined, allowing significant iron sulfide precipitation. This time-scale is representative of sulfide stress cracking (SSC) qualification tests as per NACE TM0177, which constitute one field of application of this project [14].

2. Experimental procedure

This study is part of a project of which main objective is to study the impact of oxygen pollution on SSC. Hydrogen permeation is thus used as the central experimental method, together with EIS measurements. The experimental set-up thus consists in a Devanathan-Stachurski system shown in Figure 2 [15]. The apparatus is composed of twin cells separated by the iron membrane. The cells are equipped with double jacket in order to maintain the temperature at 24 ± 2°C.

Figure 2: Experimental set up (Devanathan-Stachurski type cell).

In this experimental system, test specimens consisted in pure iron membranes, annealed under vacuum at 900 °C for 30 minutes (chemical composition provided in Table 1~~Table 1~~). These membranes were thus exposed on one side to the corrosive

environment containing H_2S where EIS measurements were made (designated as charging side), while the other side was exposed to 0.1 M sodium hydroxide and maintained at an anodic potential of 250 mV vs. Hg/HgO (1M KOH) for hydrogen permeation measurement (designated as detection side). The exit face covered by palladium following well established procedures [16]. Membrane thickness was in the order of 0.5 mm, and the exposed area was 17 cm² on both sides. Details on hydrogen permeation measurement procedure were given in a previous paper [17].

Table 1: Chemical composition of test material (mass. ppm)

EIS measurements were carried out with the iron membrane as working electrode, an Ag/AgCl reference electrode and a platinum mesh as auxiliary electrode. A perturbation of +/- 10 mV amplitude around the corrosion potential was applied with a range of frequency of 10 kHz to 1 mHz. Each EIS measurement was preceded by an open circuit potential (OCP) measurement of about 2 hours. OCP and EIS measurements were then repeated over 3 to 4 weeks. Specific precautions were taken to avoid interferences between electrochemical measurements performed simultaneously on both sides of the membrane.

In addition to the permeation membrane, pure iron flat specimens (0.9 cm x 0.9 cm x 0.05 cm) were also introduced into the charging side. These coupons were used for weight-loss corrosion rate evaluation, as well as surface analysis by scanning electronic microscopy (SEM) and X-ray diffraction (XRD). The total surface of iron

specimens exposed in the charging side was thus close to 23 cm², while the volume of test solution was 0.6 L.

Test solution at the entry side consisted in 35 g/L NaCl dissolved in distilled water. Continuous bubbling of pure H_2S was maintained during all experiments, resulting in a dissolved H_2S concentration around 0.1 M, and an initial pH around 3.8 - 4.

3. Results

Since one main goal of this study is to evaluate the evolution of H_2S corrosion over a few weeks, changes in the test solution are likely to occur. Indeed, as iron corrosion proceeded, alkalinity is released by the cathodic reaction (reduction of protons and H_2S). It results in pH increase, until iron sulfide saturation is reached. As shown on Figure 3~~Figure 3~~, initial pH corresponding to the test solution saturated with 1 bar H_2S is 3.9. After 1 day, a plateau was reached around pH 4.3 – 4.5, corresponding to FeS saturation.

Figure 3: pH evolution of test solution consisting of 35 g/L NaCl solution saturated with 1 bar H_2S at 24 °C, with iron coupons exposed to corrosion.

Typical evolution with time of exposure of Nyquist diagrams are presented in Figure 4~~Figure 4~~. For short exposure times (2 to 152 hours), Nyquist diagrams consist of a capacitive loop at high and medium frequencies, and a LF contribution which could correspond to a 45° linear tail or to the start of a second capacitive loop with a very

low characteristic frequency. Throughout all exposure period, the corrosion potential varied in a narrow range, between -690 and -700 mV vs. Ag/AgCl. These impedance diagrams are similar to those obtained by Arzola et al. [13]. In addition, and as previously observed by these authors, the diameter of the capacitive loop increases with time.

At longer immersion times, some overlap between the HF capacitive loop and the LF contribution occurs. It becomes difficult to distinguish the various contributions to the impedance, which seems to be flattened and to tend towards a single line at 45°.

Figure 4: Nyquist diagrams of pure iron exposed to a 35 g/L NaCl solution saturated with 1 bar H_2S at 24 °C for short (a) and long (b) exposure times.

Before impedance analysis, all raw experimental data were validated using Kramers-Kronig transformations. In addition, validity of impedance measurements at high frequency also had to be questioned. Indeed, at very high frequency, the impedance of the system may be simplified as the resistance of the electrolyte in series with the system capacitance (C_{HF}), corresponding to:

$$Z_{HF} \approx R_e - 1/\omega C_{HF} \qquad \text{Equation 1}$$

Code de champ modifié

Considering that the measurement noise is close to 1 %, all impedance values for which $1/\omega C_{HF}$ is lower than 1 % of R_e cannot be trusted. For our system, Re was

Code de champ modifié

close to 8 Ω and C_{HF} was initially close to 3 mF/cm² for an electrode of 16.6 cm², i.e. 45 mF. Consequently, the minimum pulsation to obtain impedance measurements above 1 % of R_e is 360 rad/s, i.e. a frequency of 57 Hz. This value is much lower than that usually considered for impedance measurements of corrosion processes. However, it is a direct consequence of the huge capacitance values obtained in the case of H_2S corrosion, resulting in a translation of impedance data to lower frequencies. The reasons for this surprisingly high capacitance value will be discussed later in the paper.

In order to determine the nature of the impedance, and to choose the model accordingly, measurements at various potentials around the corrosion potential (E_{corr}) were performed (Figure 5~~Figure 5~~). It was observed that the diameter of the HF arc decreased as the potential was more anodic, suggesting that the impedance is dominated by anodic reactions. This result will be used in the next section of the paper in order to establish the global impedance model of the system.

Figure 5: Nyquist diagram of pure iron exposed to a 35 g/L NaCl solution saturated with 1 bar H_2S at 24 °C. Measurements at E_{corr} – 50 mV, E_{corr}, and E_{corr} + 50 mV.

In addition to electrochemical measurements, flat coupons were sampled at the end of the test after 620 hours exposure. They were used for weight-loss measurements and surface analysis. Surface of the specimens was covered by a black deposit consisting mainly of mackinawite (FeS) as determined by XRD analysis. SEM

observations revealed that this surface deposit consisted of sub-micrometric plate-like crystals resulting in a highly porous scale with a thickness of 20 to 50 µm (Figure 6~~Figure 6~~). Corrosion rate, measured after removal of the deposits, was 490 µm/year.

Figure 6: SEM observation of corrosion deposits formed at iron surface after 620 hours exposure to a 35 g/L NaCl solution saturated with 1 bar H_2S at 24 ° C.

Finally, at the same time EIS measurements were carried out at the charging side of the pure iron membrane, hydrogen permeation was measured continuously by anodic extraction at the opposite side of the membrane (Figure 7~~Figure 7~~). Immediately after immersion, hydrogen permeation increases up to 60 µA/cm², followed by a slow decrease down to a plateau at 40 µA/cm², reached after a few days. Since permeated hydrogen was generated by the cathodic reaction (proton and/or H_2S reduction) during the corrosion process, it may be interesting to compare corrosion current density and hydrogen permeation current density (J_{perm}). This comparison will be carried out in the next section of the paper.

Figure 7: Hydrogen permeation for a 0.5 mm thick pure iron membrane exposed to a 35 g/L NaCl solution saturated with 1 bar H_2S at 24 °C.

4. Discussion

Impedance diagrams obtained for tests at short time immersion (Figure 4~~Figure 4~~.a) are similar to those obtained by Arzola et al. [13]. However, the equivalent circuit used by these authors corresponds to a cathodic impedance, while the results of Figure 5~~Figure 5~~ clearly indicate that the measured impedance is dominated by the anodic reactions. Consequently, impedance results were analyzed with the model of Figure 1~~Figure 1~~.a proposed in the literature to describe anodic impedance of iron corrosion in presence of H_2S [8,9]. EIS spectra fitting were carried out with SIMAD® software developed by the LISE laboratory. Curve fitting was applied to extract the various physical parameters describing the impedance of the system. Satisfactory fitting results were obtained for impedance measurements performed between 2 and 152 hours of exposure, as illustrated in Figure 8~~Figure 8~~. In order to illustrate the inconsistency of HF measurements above a few tens of Hertz, impedance data were represented after subtraction of the resistance of the electrolyte. This representation illustrates the inconsistency of HF measurements, resulting in erratic phase angles.

Figure 8: Comparisons between experimental (open symbols) and fitted impedance (lines) measured after 2 hours (a), 47 hours (b) and 152 hours (c) exposure, using the equivalent circuit of Figure 1.a.

The values of model parameters corresponding to these fitted impedances are gathered in Table 2~~Table 2~~. In order to derive capacitance values from the CPE

(constant phase elements) corresponding to the double layer capacitance used in the impedance model, the Brug's relationship was used [18,19]:

$$C_{dl} = Q^{\frac{1}{\alpha}}\left(R_e^{-1} + R_t^{-1}\right)^{\frac{\alpha-1}{\alpha}} \qquad \text{Equation 2}$$

Corrosion current densities (J_{corr}) were calculated from R_t using the Stern and Geary relationship with an anodic tafel coefficient (b_a) of 40 mV, as usually observed in H_2S environments [20] :

$$J_{corr} = b_a / 2.3R_t \qquad \text{Equation 3}$$

It must be remarked that for this type of anodic behavior with an adsorption intermediate step, the polarization resistance as determined by linear polarization or by the low frequency limit of the real part of the impedance shall not be used for corrosion rates evaluation with the Stern and Geary equation, since it does not coincide with the charge transfer resistance. For comparison, the hydrogen permeation current densities at various exposure times are also reported in Table 2~~Table 2~~.

Table 2: Component values of equivalent circuit of Figure 1.a giving the best fit of experimental impedance at various exposure times.

The most interesting fact about this analysis of impedance results at short exposure times lies in the very good match between corrosion current densities and hydrogen permeation current densities at various exposure times. Such result was, in fact, expected. Indeed, at high H_2S content and for thin steel membranes, the permeation efficiency often reaches values close to 100 %, meaning that all hydrogen produced by the cathodic reaction actually enters into the metal. This comparison also offers a direct validation of the consistency of the impedance model, confirming the validity of corrosion current density evaluation.

The other parameter which is worth examining is the double layer capacitance. It can immediately be noted that C_{dl} values exceed by at least one order of magnitude usual values for metal corrosion. It is believed that these high values are associated with the rapid formation of a conductive iron sulfide scale. Indeed, this capacitance applies to all conductive surfaces of the electrode. Consequently, it increases as the iron sulfide film is growing, and its evolution with time gives information on the true surface of the scale. At the beginning of the test, i.e. after less than a few hours immersion, its value is already quite high at 2.7 mF/cm². Since typical double-layer capacitance on metal surfaces shall be in the order of 100 µF/cm², this result implies iron sulfide scaling has already started to form, providing a high effective surface [6]. It was confirmed by visual observation that scaling was already present a few minutes after immersion. After 150 hours of exposure, the double layer capacitance reached 30 mF/cm², i.e. 300 times higher than the expected value. It can thus be inferred that the real cathodic surface reaches about 300 times that of the initially exposed iron surface. The assumption of the impact of iron sulfide scale on impedance is supported by SEM observations showing a highly porous structure offering a high effective surface (Figure 6~~Figure 6~~). Finally, it can be remarked that

the CPE coefficients are quite stable between 47 hours and 152 hours exposure, with respectively 0.73 and 0.89 for CPE_a and CPE_{dl}. The deviation from a purely capacitive behavior might be explained by 2D heterogeneities at the metal surface and by the rapid formation of the conductive iron sulfide scale. These values of α_a and α_{dl} are also in the same order as those obtained by Ma et al at various pH [8,9].

This observation of high capacitance values led us to introduce a specific component in the impedance model in order to account for the iron sulfide film. The porous electrode model was used to determine a physical model for the impedance of this conductive and porous layer iron sulfide film. According to the theory developed by de Levie [21], the impedance of a pore is given by:

$$Z_{pore} = \sqrt{R_0 Z_0}\coth\left(l\sqrt{\frac{R_0}{Z_0}}\right) \qquad \text{Equation 4}$$

where l is the pore length, R_0 is the electrolyte resistance for one-unit length pore, with units of $\Omega.cm^{-1}$, and Z_0 is the interfacial impedance (also expressed per surface unit and per unit length of the pore, with units of $\Omega.cm$). It is also common to express R_0 and Z_0 in function of the pore radius (r), and of the interfacial impedance per surface unit (Z_{eq}) as:

$$R_0 = \rho/\pi r^2 \qquad \text{Equation 5}$$

$$Z_0 = Z_{eq}/2\pi r \qquad \text{Equation 6}$$

where ρ is the electrolyte resistivity. This resistivity is considered as uniform inside all pores. Indeed, test solution contains a relatively high NaCl concentration (0.6 M) that

should be sufficient to hinder concentration gradients of reactive ions inside the pores. Another simplification made by de Levie is adopted here; i.e. that the axial concentration gradient inside the pores is negligible.

Depending on the value of *l* and *r*, the coth function in Equation 4 admits two limiting situations. If the argument is close to zero (i.e. pores with small length or large radius), then coth(*X*) is equal to 1/*X*. In such a case, Equation 4 simplifies to:

$$Z_{pore} = Z_0 / l = Z_{eq} / 2\pi r l \qquad \text{Equation 7}$$

The film behaves as a plane electrode, and its impedance is inversely proportional to the number of pores n and to the surface of pores:

$$Z_{film,plane} = Z_{pore} / n = Z_{eq} / 2n\pi r l \qquad \text{Equation 8}$$

The other limiting situation corresponds to long and thin pores, for which the argument *X* in the coth function takes high values. Then coth(*X*) tends towards 1, meaning that $Z_{pore} = \sqrt{R_0 Z_0}$. The film behaves as a semi-infinitely deep porous system, with an impedance proportional to the square root of the interfacial impedance, resulting in a 45° inclination of Nyquist plots:

$$Z_{film,porous} = \sqrt{\rho Z_{eq}} / \sqrt{2n}\pi r^{3/2} \qquad \text{Equation 9}$$

These two limiting situations correspond to model systems, for which all pores have the same geometry. In practice, and as illustrated by SEM observations of the FeS

layer, there is a distribution of pore size and geometry, leading to the co-existence of both behaviors in parallel. The total impedance of the film is then given by:

$$Z_{film}^{-1} = Z_{film,plane}^{-1} + Z_{film,porous}^{-1} \qquad \text{Equation 10}$$

As a consequence, as soon as the iron sulfide film builds-up at the metal surface, this film impedance has to be added in parallel to the faradaic contribution of Figure 1.a. The complete impedance of the system is then given by the following equivalent circuit:

Figure 9: Equivalent circuit for the corrosion of pure iron in H_2S containing environment with the formation of a conductive and porous FeS layer.

In the present case, and since the faradaic cathodic impedance is negligible (see Figure 5~~Figure 5~~), only the double layer capacitance is taken into account in the interfacial impedance Z_{eq} for both film contributions:

$$Z_{eq,*} = \frac{1}{Q_{eq,*}(j\omega)^{\alpha_*}} \qquad \text{Equation 11}$$

where* represents alternatively the parameters associated with the plane electrode or with the porous electrode contributions in the expressions of Z_{film} (Equations 8 to 10).

Although it may seem quite complicated, this impedance model still presents several simplifying assumptions. First, as in the original development of the transmission line model by de Levie, it is considered that the ohmic drop along the pores is negligible. It is also considered that there is no axial concentration gradient inside the pores. Then, in the expression used for the film impedance (Equation 10), the pores where the coth term plays a role (i.e. different from the two limiting cases described above) are neglected. It means that equation 10 correctly represents situations where the iron sulfide film behaves as a plane electrode or as a porous electrode, or both in parallel. But it presents some weaknesses when the pores geometry is so that simplifications of the coth function are not valid (i.e. argument value is neither close to zero nor close to infinite). A more robust approach to describe the impedance of this film would consist in considering a distribution of pore sizes. This type of approach is often used for energy storage applications, where porous electrodes are used to maximize current densities [22–25]. Equivalent circuit approaches then becomes inappropriate, and numerical resolutions are required. The validity of these assumptions will be further discussed after comparing electrochemical data with weight-loss and hydrogen permeation measurements, at the end of this paper.

The model was then used to analyze impedance spectra obtained at various immersion times. For short immersion times, when the iron sulfide film is thin with relatively large pores, it was found that the film impedance is only composed of $Z_{film,plane}$, i.e. a purely capacitive contribution. This film capacitance being in parallel with the double layer capacitance of the initial model of Figure 1.a, the equivalent circuit is fully equivalent to the circuit of Figure 1.a (provided that CPE coefficients are not too different). Introduction of the iron sulfide film contribution thus provides a

physical explanation for the high values of capacitance determined during the analysis of the results at short exposure times.

For longer exposure times, the model comprising only $Z_{film,plane}$ did not give consistent results anymore. In particular, the coefficient for the CPE contribution drastically decreased to values close to 0.5, which does not have physical significance. It was then necessary to introduce the porous film contribution $Z_{film,porous}$ in order to explain the inclination of Nyquist plots close to 45°. The complete model with both film contributions (Figure 9~~Figure 9~~) was then used to analyze impedance results at longer exposure times. However, due to the high number of adjustable parameters, excellent fitting results could be obtained with various sets of parameters. It was thus necessary to fix several parameters at constant values. In particular, both CPE coefficients were set at 0.73 (CPE_a) and 0.89 (CPE_{plane}), i.e. at the same values as determined for short exposures. In addition, the charge transfer resistance was restrained to the range 400 – 500 Ω.cm². Illustrations of fitting accuracy are given in Figure 10~~Figure 10~~, for the experimental data obtained after 437 and 572 hours.

Mis en forme : Police :(Par défaut) Arial, 12 pt, Anglais (États-Unis)

Figure 10: Comparisons between experimental (open symbols) and fitted impedance (lines) measured after 437 hours (a) and 572 hours (b) exposure, using the equivalent circuit of Figure 9~~Figure 9~~.

Mis en forme : Police :(Par défaut) Arial, 12 pt, Anglais (États-Unis)

Eventually, the evolutions with time of R_t and J_{corr} over the entire exposure time are plotted on Figure 11~~Figure 11~~. Hydrogen permeation current density (J_{perm}) is also plotted for comparison.

Figure 11: Comparison of J_{perm} with J_{corr} determined from R_t values determined by EIS fitting with the model of Figure 9~~Figure 9~~.

Mis en forme : Police :(Par défaut) Arial, 12 pt, Anglais (États-Unis)

As already mentioned, the similarity between corrosion and permeation current densities is remarkable. The permeation efficiency is maintained at values close to 100 % even at longer exposure times. In addition, and considering the total time of exposure, an average corrosion current density of 45 µA/cm² was obtained, corresponding to a corrosion rate of 530 µm/year. This value is in very good agreement with weight loss measurements performed on small coupons, exhibiting a corrosion rate of 490 µm/year. This result also confirm that it was reasonable to restrain R_t values in the range 400 – 500 Ω.cm² when fitting impedance obtained at long exposure times. This good correlation also validates the simplifying hypothesis describes above, at least for the determination of R_t, which is the only parameter used for the analysis of corrosion.

It can finally be noted that the new model proposed in this paper is consistent with literature data, while giving new insights in unexplained results from the literature. For short immersion times, when no film formation occurs or when the iron sulfide film remains sufficiently thin, the film behaves as a pure capacitance. It results in high values of capacitance, while the faradaic contribution is dominated by the anodic reactions with an adsorbed intermediate, as proposed by Ma et al. [8,9]. The same

model also allows representing the results of Veloz et al. [11], and it gives a physical explanation for the high capacitance values obtained in this paper.

For longer exposure times, a flattening of impedance diagrams is observed, tending towards a 45° line. For this system, where impedance is dominated by the anodic reactions and for which the reactive species are available at high concentration in the solution, diffusion limitation is unlikely to take place. The porous electrode behavior, associated with the conductive iron sulfide scale that forms at the electrode surface, gives a physical explanation for observed impedance.

5. CONCLUSION

Corrosion of pure iron in H_2S saturated 35g/L NaCl solution was studied for 3 to 4 weeks. An impedance model was proposed, with two distinct contributions: i/ a faradaic anodic impedance consisting of a two-step reaction with charge transfer and adsorption – desorption and, ii/ the impedance of the conductive and highly porous iron sulfide (mackinawite) film. This impedance model is fully compatible with previous proposals of the literature, and its physical meaning is now well established, which was not completely available yet in the case of film formation. The main impact of this scale is to induce extremely high values of double-layer capacitance, due to the huge increase of effective surface which can reach nearly 600 times that of the geometrical surface of the metallic electrode.

The analysis of impedance data also allowed determining the evolution with time of the charge transfer resistance, from which the corrosion current density could directly be estimated. Corrosion rates evaluated from impedance data were perfectly correlated with weight loss measurements. It was also found that corrosion current density was nearly identical to the hydrogen permeation current density over the

whole duration of the tests. This permeation efficiency of 100 % was expected in our test conditions, i.e. high H_2S content and thin metal membrane. Therefore, hydrogen permeation provides a direct and independent measurement of the cathodic current density, also corresponding to the corrosion current density.

This impedance model will now be used to study the impact of environmental parameters on iron corrosion in H_2S environment. In the second part of this paper, a study of the effect of continuous ingress of oxygen in the H_2S environment will be proposed.

Acknowledgements

The authors kindly thank Alexandre Bonneau for his participation in the implementation of the experimental setup. Remy Mingant is also warmly acknowledged for his active participation in the analysis and modeling of impedance data. The contribution of IFPEN analysis department in the surface characterization and test solution analysis is also greatly acknowledged.

References

[1] P. Altoé, G. Pimenta, C.F. Moulin, S.L. Díaz, O.R. Mattos, Evaluation of oilfield corrosion inhibitors in CO_2 containing media: A kinetic study, Electrochim. Acta 41 (1996) 1165.

[2] D.S. Carvalho, C.J.B. Joia, O.R. Mattos, Corrosion rate of iron and iron-chromium alloys in CO_2 medium, Corros. Sci. 47 (2005) 2974.

[3] T. Almeida, M.C.E. Bandeira, R.M. Moreira, O.R. Mattos, New insights on the role of CO_2 in the mechanism of carbon steel corrosion, Corros. Sci. 120 (2017) 239.

[4] K.L.J. Lee, S. Nesic, The effect of trace amount of H_2S on CO_2 corrosion investigated by using EIS technique, in: Corrosion 2005, Houston, TX (USA) 3-7 April 2005, paper 630, NACE International.

[5] K.L.J. Lee, S. Nesic, EIS investigation of CO_2/H_2S corrosion, in: Corrosion 2004, New-Orleans, LO (USA) March 28 - April 1 2004, paper 728, NACE International.

[6] D.C. Grahame, The electrical double layer and the theory of electrocapillarity, Chem. Rev. 41 (1947) 441.

[7] C. Gabrielli, M. Keddam, B.D. Cahan, C.T. Chen, The Nature of the Passive Film on Iron .2. Ac Impedance Studies, J. Electrochem. Soc. 129 (1982) 2872.

[8] H.Y. Ma, X.L. Cheng, G.Q. Li, S.H. Chen, Z.L. Quan, S.Y. Zhao, L. Niu, The influence of hydrogen sulfide on corrosion of iron under different conditions, Corros. Sci. 42 (2000) 1669.

[9] H.Y. Ma, X.L. Cheng, S.H. Chen, G.Q. Li, X. Chen, S.B. Lei, H.Q. Yang, Theoretical interpretation on impedance spectra for anodic iron dissolution in acidic solutions containing hydrogen sulfide, Corrosion 54 (1998) 634.

[10] M.E. Orazem, B. Tribollet, Electrochemical impedance spectroscopy, Wiley ed., The Electrochemical Society Series (2017), 2nd edition.

[11] M.A. Veloz, I. González, Electrochemical study of carbon steel corrosion in buffered acetic acid solutions with chlorides and H_2S, Electrochim. Acta 48 (2002) 135.

[12] H.H. Tang, M.S. Cayard, Test methods for the evaluation of materials for wet H2S service, in: Corrosion/99, San Antonio, TX (USA) 25-30 April 1999, NACE International.

[13] S. Arzola, J. Genescá, The effect of H_2S concentration on the corrosion behavior of API 5L X-70 steel, J Solid State Electrochem. 9 (2005) 197.

[14] NACE TM0177-2016, Laboratory Testing of Metals for Resistance to Sulfide Stress Cracking and Stress Corrosion Cracking in H2S Environments, NACE International, Houston, TX (USA).

[15] M.A.V Devanathan and Z. Stachurski, The mechanism of hydrogen evolution on iron in acid solutions by determination of permeation rates, J. Electrochem. Soc. 111 (1962) 619.

[16] P. Manolatos, M. Jerome, J. Galland, Necessity of A Palladium Coating to Ensure Hydrogen Oxidation During Electrochemical Permeation Measurements on Iron, Electrochim. Acta 40 (1995) 867.

[17] M. D. Deffo-Ayagou J. Kittel, C. Mendibide, C. Duret-Thual, N. Ferrando, E. Sutter, M. Tran, B. Tribollet, Corrosion of Pure iron and Hydrogen Permeation in the Presence of H2S with O_2 contamination, in: Corrosion 2018 Phoenix, AZ (USA) 15-19 April 2018, paper 10931, NACE International.

[18] R. de Levie, Electrochemical response of porous and rough electrodes, in. Paul Delahay (Ed.), Advances in Electrochemistry and Electrochemical Engineering, volume 6 (1967) 329.

[19] B. Hirschorn, M.E. Orazem, B. Tribollet, V. Vivier, I. Frateur, M. Musiani, Determination of effective capacitance and film thickness from constant-phase-element parameters, Electrochim. Acta 55 (2010) 6218.

[20] G.J. Brug, A.L.G. van den Eaden, M. Sluyters-Rehbach, J.H. Sluyters, The analysis of electrode impedances complicated by the presence of a constant phase element, J. Electroanal. Chem. 176 (1984) 275.

[21] Y. Zheng, Electrochemical mechanism and model of H_2S corrosion of carbon steel, PhD Dissertation, The Russ College of Engineering and Technology of Ohio University, 2015.

[22] J. Huang, J. Zhang, Theory of Impedance Response of Porous Electrodes, J. Electrochem. Soc. 163 (2016) A1983.

[23] R. Kant, M.B. Singh, Theory of the Electrochemical Impedance of Mesostructured Electrodes Embedded with Heterogeneous Micropores, J. Phys. Chem. C 121 (2017) 7164.

[24] A. Lasia, Impedance of porous electrodes, Journal of Electroanalytical Chemistry 397 (1995) 27.

[25] H.-K. Song, Y.-H. Jung, K.-H. Lee, H. Le Dao, Electrochemical impedance spectroscopy of porous electrodes: the effect of pore size distribution, Electrochimica Acta 44 (1999) 3513.

a)

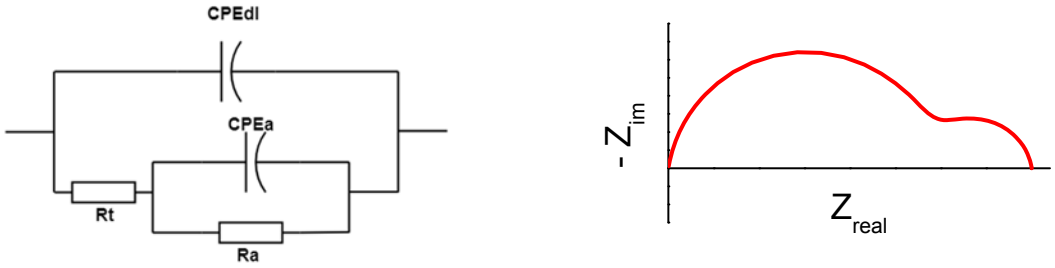

b)

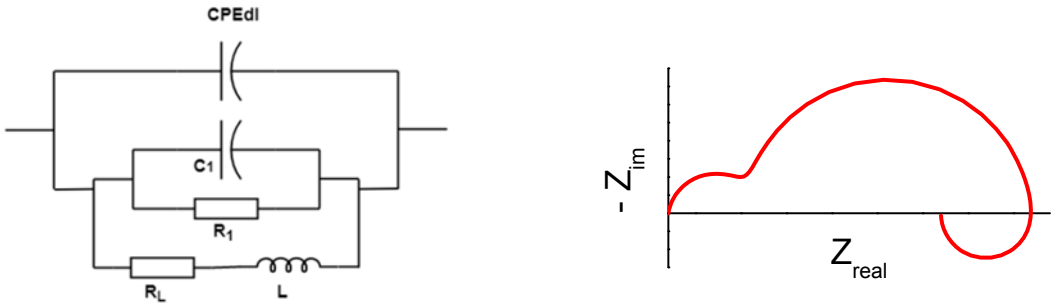

c)

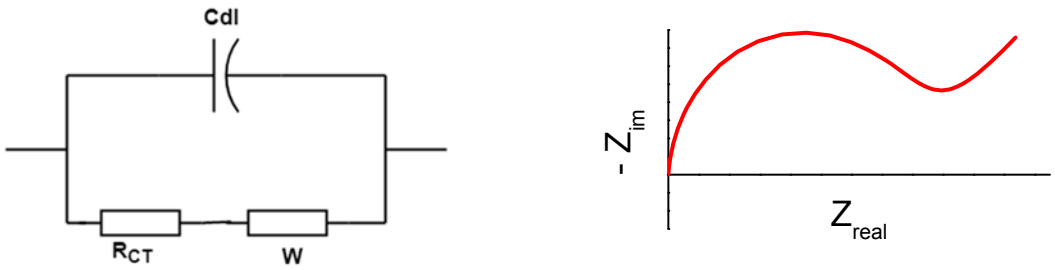

Figure 1: Equivalent circuits and corresponding impedance diagram used in the literature to describe iron corrosion in presence of H_2S [8,9,13]. For the sake of simplicity, electrolyte resistance was removed from these equivalent circuits.

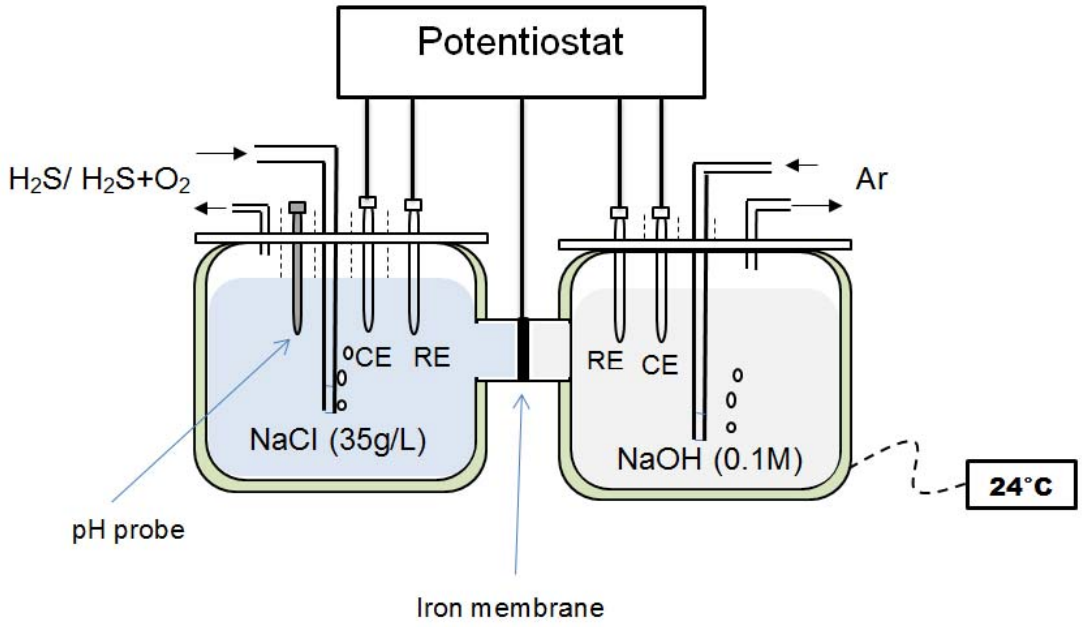

Figure 2: Experimental set up (Devanathan-Stachurski type cell).

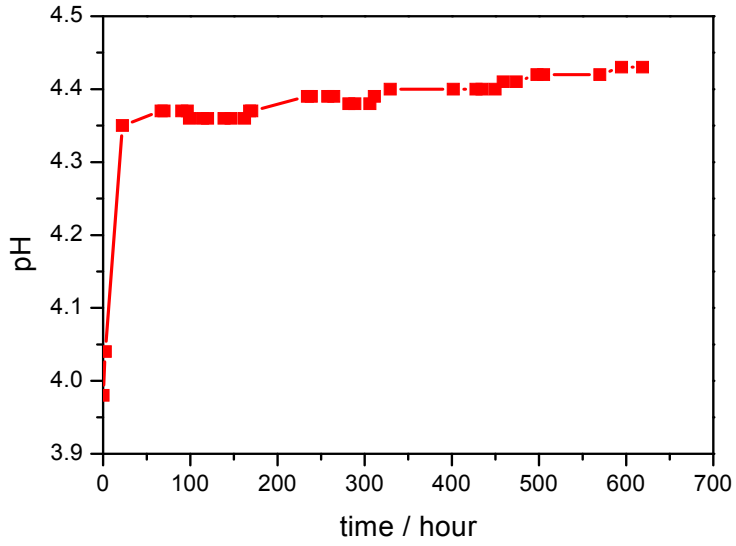

Figure 3: pH evolution of test solution consisting of 35 g/L NaCl solution saturated with 1 bar H_2S at 24 °C, with iron coupons exposed to corrosion.

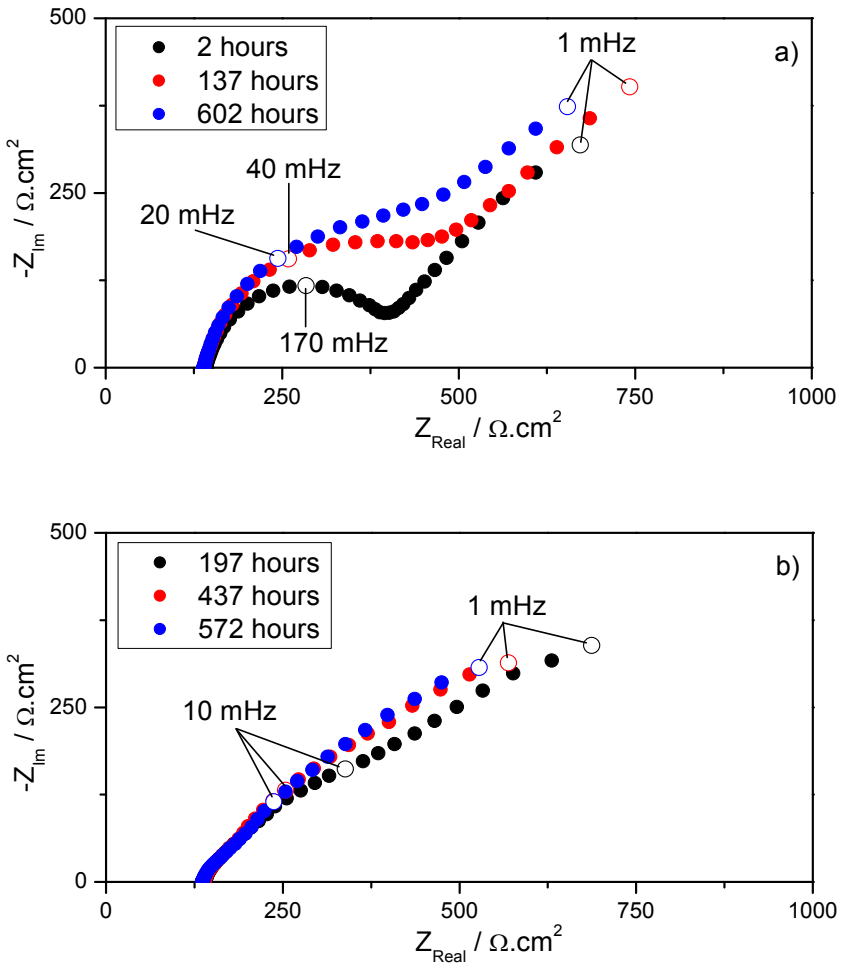

Figure 4: Nyquist diagrams of pure iron exposed to a 35 g/L NaCl solution saturated with 1 bar H_2S at 24 °C for short (a) and long (b) exposure times.

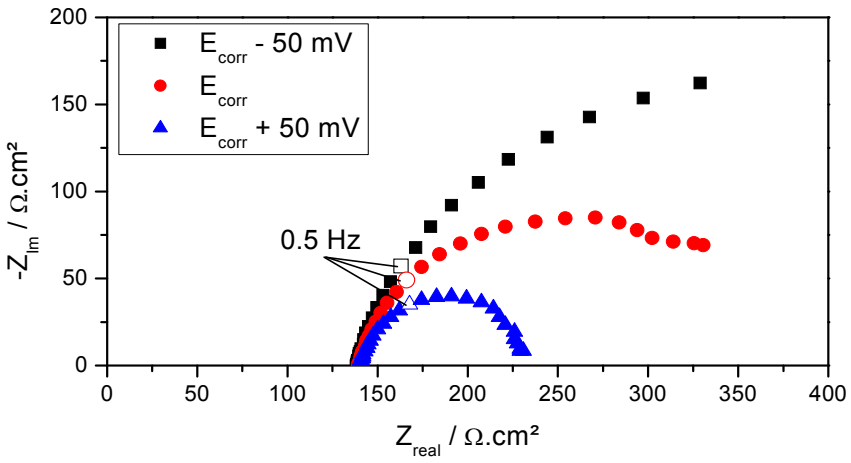

Figure 5: Nyquist diagram of pure iron exposed to a 35 g/L NaCl solution saturated with 1 bar H_2S at 24 °C. Measurements at E_{corr} – 50 mV, E_{corr}, and E_{corr} + 50 mV.

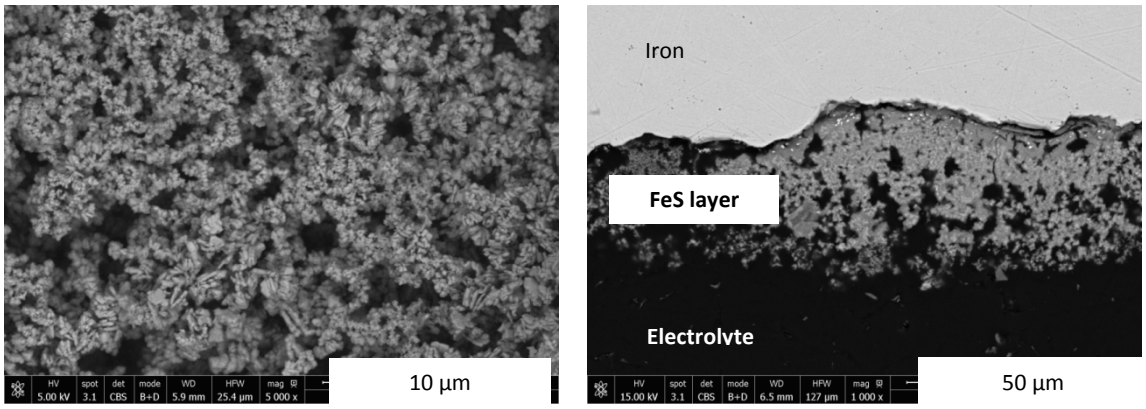

Figure 6: SEM observation of corrosion deposits formed at iron surface after 620 hours exposure to a 35 g/L NaCl solution saturated with 1 bar H_2S at 24 ° C.

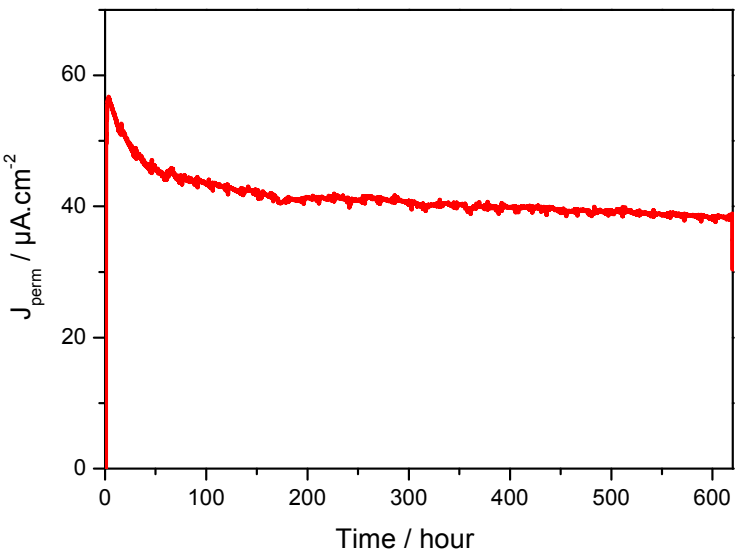

Figure 7: Hydrogen permeation for a 0.5 mm thick pure iron membrane exposed to a 35 g/L NaCl solution saturated with 1 bar H_2S at 24 °C.

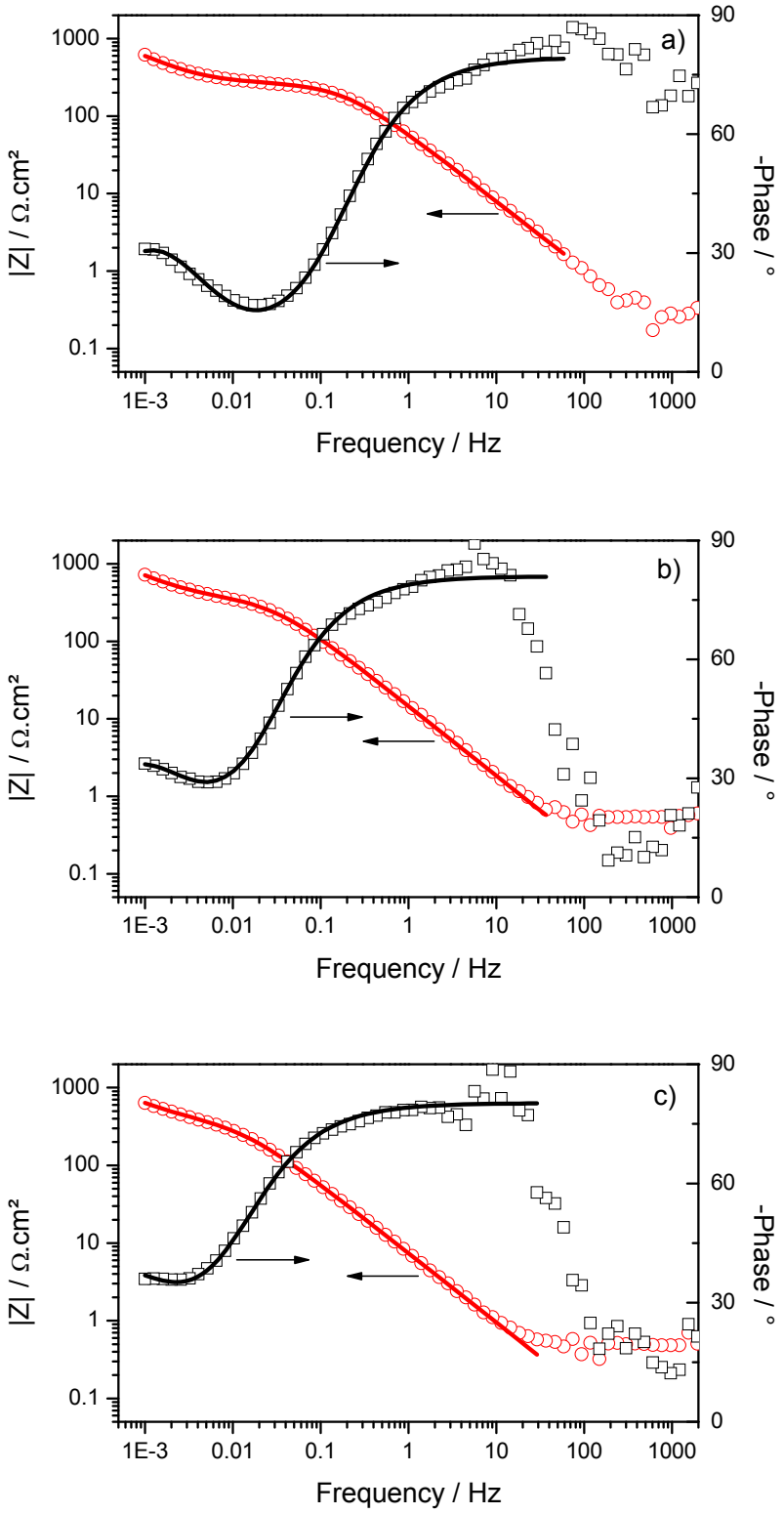

Figure 8: Comparisons between experimental (open symbols) and fitted impedance (lines) measured after 2 hours (a), 47 hours (b) and 152 hours (c) exposure, using the equivalent circuit of Figure 1.a.

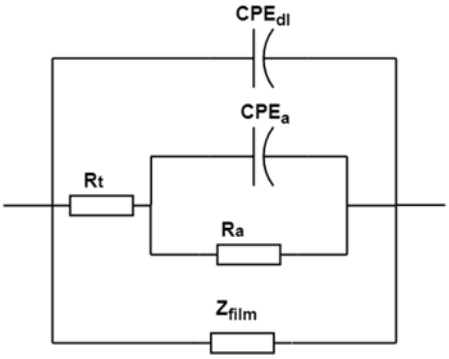

Figure 9: Equivalent circuit for the corrosion of pure iron in H_2S containing environment with the formation of a conductive and porous FeS layer.

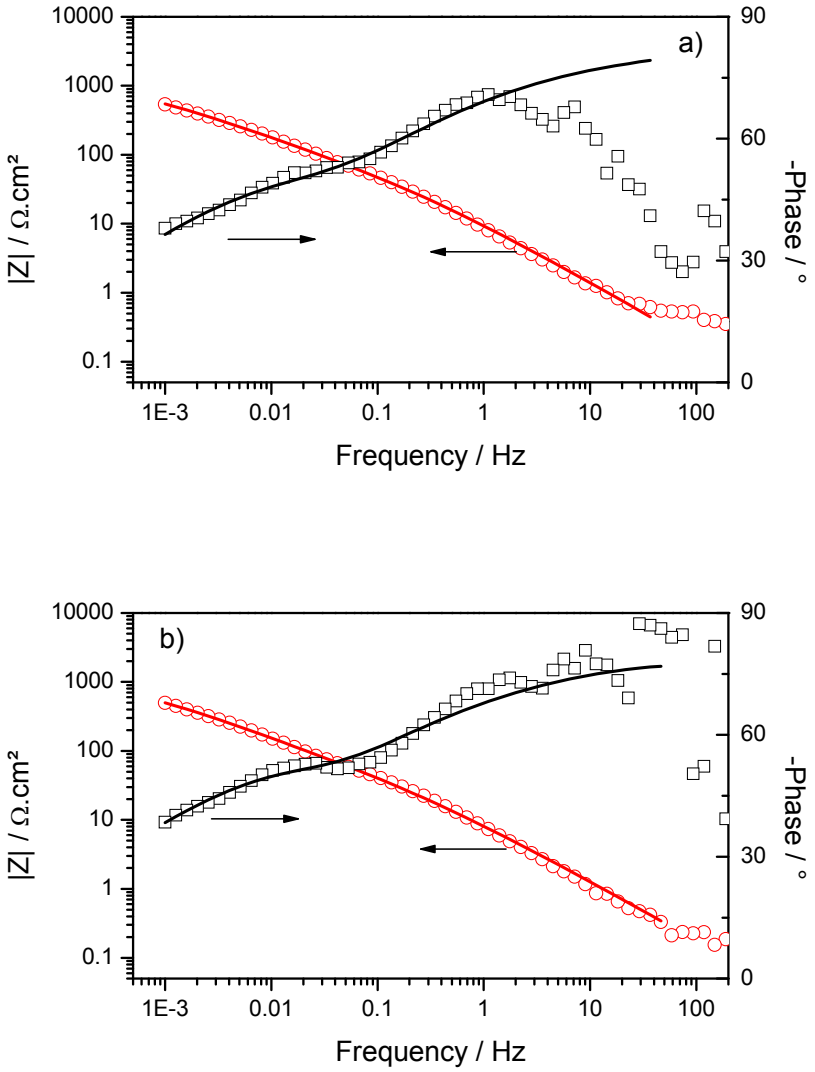

Figure 10: Comparisons between experimental (open symbols) and fitted impedance (lines) measured after 437 hours (a) and 572 hours (b) exposure, using the equivalent circuit of **Erreur ! Source du renvoi introuvable.**.

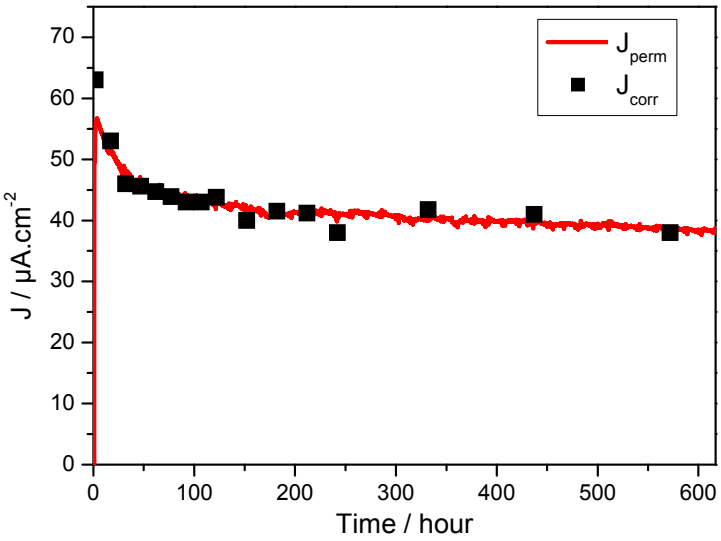

Figure 11: Comparison of J_{perm} with J_{corr} determined from R_t values determined by EIS fitting with the model of **Erreur ! Source du renvoi introuvable.**.

Table 1: Chemical composition of test material (mass. ppm)

Al	Cr	Cu	Mn	Ni	Si	Ti	C	P	S	Fe
107	133	55	240	159	100	5	18	60	48	Bal

Table 2: Component values of equivalent circuit of Figure 1.a giving the best fit of experimental impedance at various exposure times.

	2 hours	47 hours	152 hours
R_e (Ω.cm²)	143	140	139
Q_a	0.13	0.09	0.09
α_a	0.78	0.74	0.73
R_a (Ω.cm²)	910	1594	3202
Q_{dl}	0.003	0.013	0.026
α_{dl}	0.89	0.90	0.89
C_{dl} (mF.cm^{-2})	2.6	13.4	29.4
R_t (Ω.cm²)	276	381	435
J_{corr} (µA.cm^{-2})	63	46	40
J_{perm} (µA.cm^{-2})	55	46	42